

# Hide and seek with a Neutron Star

## Hint of Neutron Star activity in SN 2015ap light curve

Fabio Ragosta<sup>1,2</sup>, Giulia Illiano<sup>3</sup>, Andrea Simongini<sup>4</sup>, Matteo Imbrogno<sup>3</sup>, Silvia Piranomonte<sup>3</sup>, and Andrea Melandri<sup>3</sup>,

<sup>1</sup> Dipartimento di Fisica “Ettore Pancini”, Università di Napoli Federico II, Via Cinthia 9, 80126 Naples, Italy  
e-mail: E-mail: [fabio.ragosta@unina.it](mailto:fabio.ragosta@unina.it)

<sup>2</sup> INAF - Osservatorio Astronomico di Capodimonte, Via Moiariello 16, I-80131 Naples, Italy

<sup>3</sup> INAF, Osservatorio Astronomico di Roma, Via di Frascati 33, I-00078 Monteporzio Catone, Italy

<sup>4</sup> Università Tor Vergata, Dipartimento di Fisica, Via della Ricerca Scientifica 1, I-00133 Rome, Italy

### ABSTRACT

**Aims.** We present a detailed study of the unique SN 2015ap, a very energetic event, notable for its exceptionally high bolometric peak magnitude if compared to other well-know Type Ib supernovae. We analyzed its multi-wavelength light curve, which exhibited a possible period modulation that could result from a geometrical effect.

**Methods.** We analyzed the modulation present at all available bands in SN 2015ap’s light curves using a Bayesian approach for measuring the period of variability. Additionally, narrow  $H_\alpha$  emission is observed in late-time spectra, exhibiting periodic velocity shifts likely originating from hydrogen gas stripped from a companion and accreted onto the compact remnant.

**Results.** We propose that SN 2015ap’s significant light curve modulation arise from accretion onto a neutron star as the remnant of SN 2015ap. Our multi-wavelength observations reveal a sinusoidal modulation with a period of 8.4 days, confirmed by periodic variations in the  $H_\alpha$  emission lines. Traditional models of circumstellar medium interactions cannot account for these features due to the unusually high ejection rates required. Using the Taylor-Spruit dynamo model, we suggest that the interaction between accreting matter and the neutron star’s magnetosphere could account for the observed periodic modulation. This implies assuming an ejecta-companion interaction because the accretion from fallback ejecta alone would not produce the observed modulation. The binary configuration, characterized by a separation of less than  $50 R_\odot$ , supports a magnetized neutron star central engine as the primary mechanism, rather than models involving circumstellar material interaction.

**Key words.** Neutron Stars - Supernovae - Extragalactic - Compact Object

## 1. Introduction

Supernovae (SNe) are among the most spectacular events in the Universe. These stellar explosions release an enormous amount of kinetic energy ( $\approx 10^{51}$  erg), out of which about  $\approx 10^{49}$  erg is emitted as radiation and are visible for a short time (several weeks to months) before fading from view. In particular, stars with zero-age main sequence masses  $M_{ZAMS} \geq 8 M_\odot$  end their lives as Core-Collapse Supernovae (CCSNe), which rank among the most powerful stellar explosions. Extensive observations of this kind of transients have led to a detailed classification system based on their light curve and spectral features (see review by Filippenko 2005). The diversity in observable properties of these SNe depends on the progenitor star’s initial mass, metallicity, binarity, and mass-loss history. The classification of CC-SNe is based on both the morphology of the bolometric light curve and the presence of specific lines in the spectra during their evolution. SNe showing prominent hydrogen (H) features are classified as Type II, while those lacking them fall into Type I. These primary categories are further divided into various subclasses: Type Ib SNe exhibit prominent helium (He) features in their spectra, whereas Type Ic SNe show neither H nor He obvious features. Separately, Type Ia SNe—though not core-collapse supernovae—are distinguished by the presence of a strong sili-

con II (SiII) feature in their spectra, as they originate from the thermonuclear explosion of a white dwarf.

Prominent features of intermediate-mass elements such as oxygen, magnesium, and calcium are seen both in Type Ib and Ic SN spectra (see Gal-Yam 2017, for a general introduction). Although SNe Ib/c lack obvious H features in their early-time spectra, few studies have focused on the existence of H in some of SNe Ib at later time (e.g., Branch et al. 2002; Elmhamdi et al. 2006; Kuncarayakti et al. 2023; Agudo et al. 2023).

In the post-photospheric phase, when the SN ejecta become optically thin, the light curves of CCSNe are powered by energy deposition from the radioactive decay of  $^{56}\text{Co}$  and  $^{56}\text{Fe}$ . In many cases, the SN progenitor is surrounded by dense circumstellar matter (CSM), leading to a violent interaction between the SN ejecta and the CSM during the explosion. This interaction produces forward and reverse shock, which transfer their kinetic energy into the surrounding material. This energy is then radiatively released, powering the light curve (e.g., Chevalier 1982; Arnett 1982; Chevalier & Fransson 1994; Moriya et al. 2011; Chatzopoulos et al. 2013a; Guillochon et al. 2018; Srinivasaragavan et al. 2024). Some SNe Ib (e.g, Maeda et al. 2007a; Kasen et al. 2016; Liu et al. 2021; Zhang et al. 2022) have also shown features that may suggest an injection of energy from a young magnetar (e.g., Ostriker & Gunn 1969; Arnett & Fu 1989;

Maeda et al. 2007b; Kasen & Bildsten 2010; Woosley 2010; Chatzopoulos et al. 2013a; Nicholl et al. 2017a)

All the studies cited above have almost been exclusively focused on single stellar progenitors. However, there are many indications that massive stars form mainly as members of binary or higher-order systems (e.g., Chini et al. 2012; Sana et al. 2014; Sugimura et al. 2020), and many of them have close enough orbital separations for the stellar companion components to interact during their evolution (e.g., Sana et al. 2012; Schneider et al. 2014). Thus, it is expected that the majority of CCSNe occur in massive close binaries. The evolution of a star in a binary system through mass transfer, mass loss, and merging modifies the binary population. When the primary star explodes, the binary can become unbound due to either mass loss or ‘kicks’ imparted by the explosion (e.g., De Cuyper 1982).

Binary evolution is commonly required to explain the high intrinsic rate of hydrogen poor (type Ib, Ib, Ic) CCSNe (e.g., Podsiadlowski et al. 1992; Eldridge et al. 2008; Yoon et al. 2010; Claeys et al. 2011; Zapartas et al. 2017; Sravan et al. 2020; Shivvers et al. 2022) and their ejecta mass distributions peaked at low values of about  $2 M_{\odot}$  (e.g., Lyman et al. 2016; Taddia et al. 2018). It is also required to explain the properties of several SNe observed through direct imaging, including the triple-ring structure of SN 1987A (e.g., Eldridge et al. 2015, 2017; Utrobin et al. 2021).

Recently, Moore et al. (2023) and Chen et al. (2024b) presented the first evidence of a modulation in the radioactive decay tail for SN 2022jli. In one of the proposed scenarios, the authors suggest that the modulation arises from mass transfer from a companion star onto the newly formed neutron star (NS). Furthermore, the periodicity observed in the light curve, along with narrow  $H_{\alpha}$  emission lines and consistent  $\gamma$ -ray emissions, strongly supports this interpretation. The 12.4-day modulation likely reflects the orbital period of the binary system, providing a direct link between the binary interaction and the observed modulation. Chen et al. (2024b) suggest that the energy powering the light curve, including the  $\gamma$ -ray emission, results from the accretion process, where the mass inflow fuels extreme luminosities that surpass the Eddington limit. This phenomenon highlights the significant role of binary systems in shaping supernova remnants and producing distinctive observational signatures.

In this paper, following the unique case of SN 2022jli, we apply a similar analysis investigating for modulations to the interesting case of SN 2015ap (Aryan et al. 2021), a very energetic SN Ib (Ross et al. 2015; Gangopadhyay et al. 2020).

## 2. Data

SN 2015ap was discovered on 2015 September 8 by the 0.76-m Katzman Automatic Imaging Telescope (KAIT; Li et al. 2000) as part of the Lick Observatory Supernova Search (LOSS; Filippenko et al. 2001) in an unfiltered 18 s image (Ross et al. 2015). Its host galaxy IC 1776 has a redshift of  $z = 0.011375 \pm 0.000017$  (Chengalur et al. 1993) and a barred spiral morphology. The SN was classified as a type Ib a few days after maximum brightness on the basis of well-developed features of He I, Fe II, and Ca II (Gangopadhyay et al. 2020).

Photometric and spectroscopic data for SN 2015ap were collected from public release available in Guillochon et al. (2017); Aryan et al. (2021); Roming et al. (2005); Brown et al. (2014); Prentice et al. (2018a); Yaron & Gal-Yam (2012) as detailed in Appendix A. Extinction corrections were applied using values from Schlafly & Finkbeiner (2011). The quasi-bolometric light curve was derived using the `superbol` code (Nicholl

2018), fitting blackbody models to extinction-corrected data. The peak quasi-bolometric luminosity, calculated over the wavelength range  $4000 - 10000 \text{ \AA}$ , is  $\log F = 43.37 \pm 0.02$ , higher than what measured by Prentice et al. (2018a). For the epoch of maximum brightness in the B band, we adopted the estimate by Aryan et al. (2021):  $T_{\text{max}} = 57282.47 \pm 2.56 \text{ MJD}$ . The morphology and properties of the light curve are described in detail in Gangopadhyay et al. (2020).

The spectra reveal prominent features of He I, Mg II, Fe II, Si II, and O I, consistent with the properties of Type Ib SNe. The He I 5876  $\text{\AA}$  line shows an expansion velocity of approximately  $15,500 \text{ km s}^{-1}$ , characteristic of stripped-envelope supernovae.

## 3. Analysis

The results in Moore et al. (2023) suggested that the effect of the presence of a binary companion should be also observable in the light curve evolution of SN 2015ap. Hence, following Moore et al. (2023), we performed a similar analysis to search for periodicity in the multi-wavelength light curves and multi-epoch spectra of SN 2015ap.

### 3.1. Photometric evolution

SN 2015ap photometry has already been broadly analyzed in the literature, and data from Swift, KAIT, LCO, and other facilities can be easily found publicly. As stated in Appendix A, we used publicly available data which cover UW1-, UW2-, UM2-, U-, u-, B-, V-, g-, R-, r-, I-, i-bands (see Fig. 1). The evolution of the SN 2015ap appears very typical, with a rapid rise in the UV band and a decreasing count rate in the redder bands. The rising phase of the light curve in UV, near-UV bands is steeper than in typical supernovae. This can be explained by the injection of more energetic photons during the early stages of the evolution. We could interpret this finding as due to the presence of an additional energy source beyond the Ni-decay mechanism.

The absence of a plateau phase suggested that the effect of a CSM, if present, is negligible, thus, we inspect the model suggested in (Moriya et al. 2015), which assumes, instead, the presence of a low-density inflated envelope due to evolution of the star near its Eddington luminosity.

#### 3.1.1. Bolometric light curve.

To derive the pseudo-bolometric light curve, we integrated the observations in the UW1-, UW2-, UM2-, U-, u-, B-, V-, g-, R-, r-, I-, i-bands using the publicly available code `superbol` (Nicholl 2018). The corresponding peak luminosity is  $L_{\text{opt}} = 10^{43.5 \pm 0.02} \text{ erg s}^{-1}$ , which is within the typical range of Stripped Envelope SNe found by Taddia et al. (2018) and Prentice et al. (2018a). The total integrated luminosity (through the wavelength range  $2600 - 8600 \text{ \AA}$ ) is  $E_{\text{opt}} \approx 7.4 \times 10^{49} \text{ erg}$ .

The bolometric luminosity derived here is almost two orders of magnitude higher than the one measured in (Aryan et al. 2021). This is because we considered in our estimation the contribution of the UV bands, which is not negligible in the rising phase. The effect of these bands was not previously considered, underestimating the bolometric luminosity.

Unexpectedly, the bolometric evolution of SN 2015ap showed a clear bump on the tail, at which can be noted an increase in the temperature and no change of ejecta radius (see Figure 2).

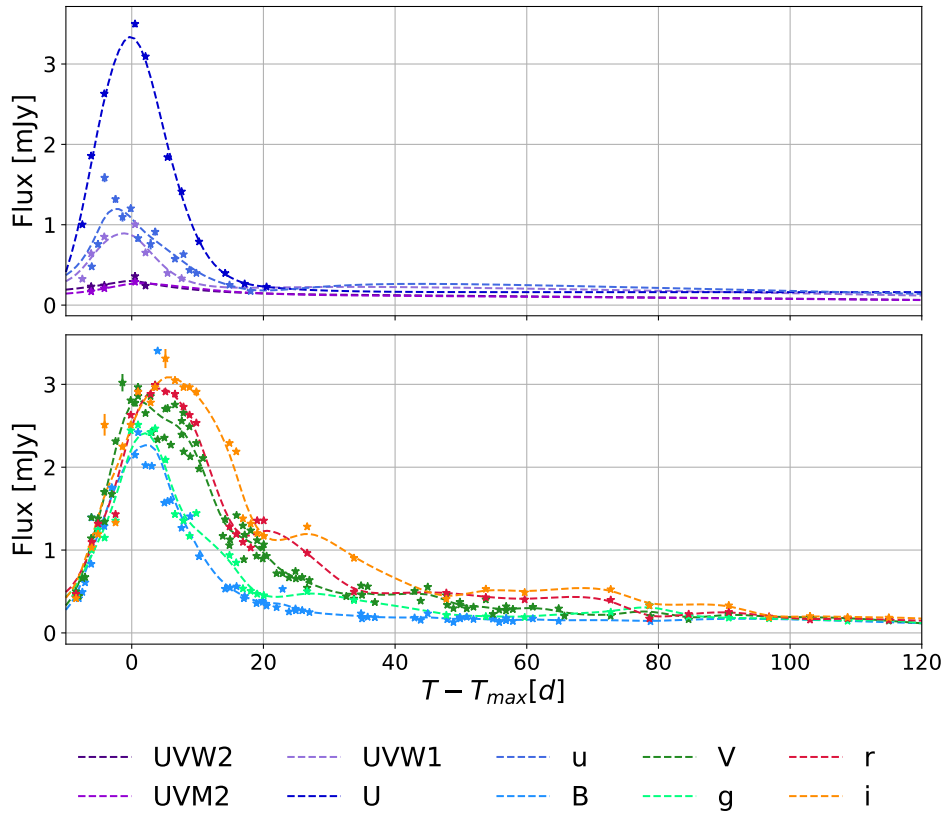


**Fig. 1.** Multi-wavelength light curves of SN 2015ap. For more details on the analysis, the reader can refer to Sect. 3. The dashed lines are the Gaussian Process representation of the light curves in each filter.

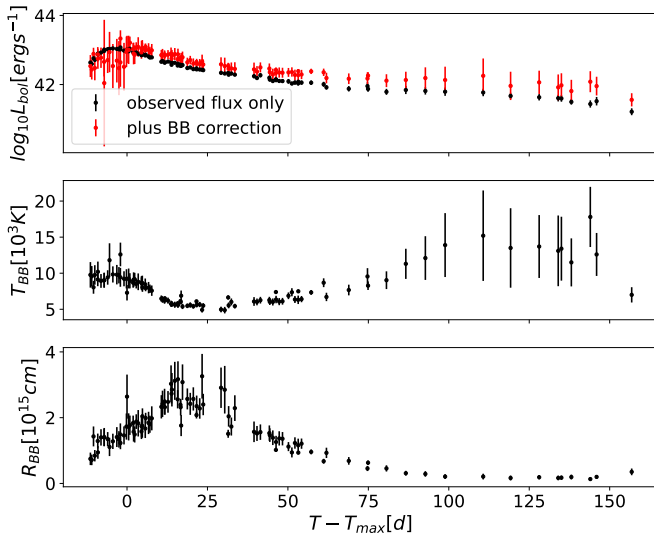


**Fig. 2.** Results of bolometric light curve estimation using *superbol*. Top panel: comparison between pseudobolometric observed light curve, integrated trapezoidally, and bolometric light curve including the additional BB corrections; middle panel: evolution of the estimated black body temperature with time from maximum of bolometric light curve; bottom panel: evolution of the estimated black body radius with time from maximum of bolometric light curve.

The bump is also reflected in the color evolution (Fig. 3), which shows an initial blueward trend corresponding to the ris-

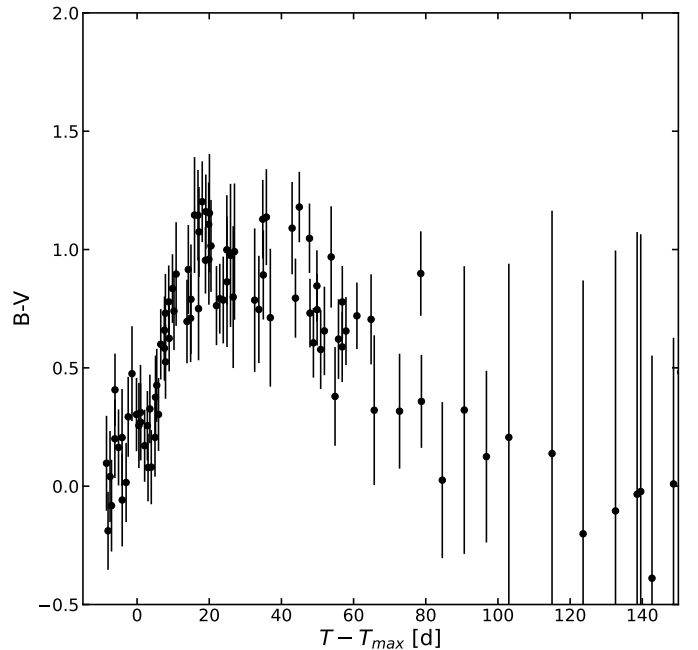


**Fig. 3.** B-V color evolution of SN 2015ap.

ing phase of the photometric evolution. The observed trend then reverses for  $\sim 40$  days, after which a steep shift back toward the blue part of the spectrum is marked by a second peak. Typically this second peak is not expected to be so pronounced if the temperature increase is interpreted as due to CMS interaction. Even-

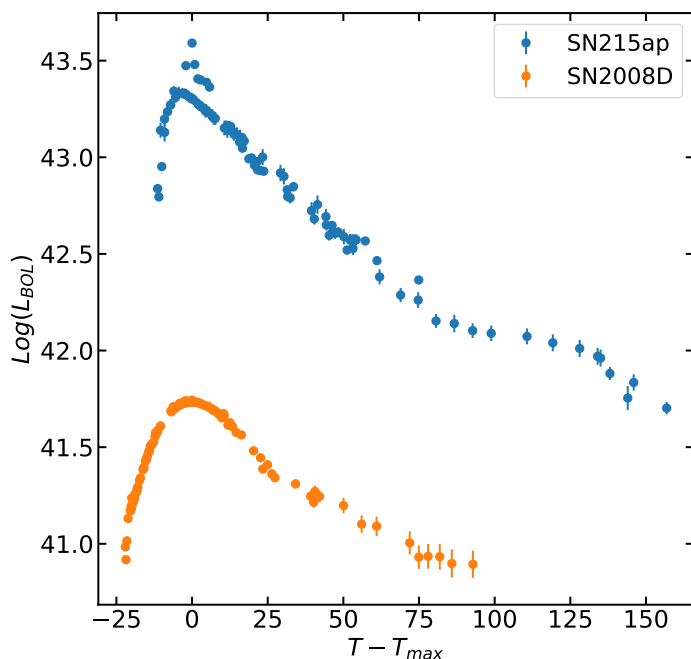


**Fig. 4.** Comparison between SN2008D and SN 2015ap bolometric light curves.

tually, the rapid temperature variation and the non-linear evolution of the B-v color curve, suggest the presence of a prolonged breakout phase and, thus, a progenitor with an inflated envelope

A similar effect has been observed in SN 2008D, supporting the idea that some progenitor stars may develop inflated envelopes before exploding due to their high luminosity. One consequence of this is that less material falls back onto the remnant, which can favor the formation of a NS rather than a black hole. The prolonged breakout phase and the presence of bumps in the late-time light curve may, therefore serve as indirect evidence of NS formation. A comparison with SN 2008D showed that SN 2015ap has a steeper evolution of the rising part of the early evolution of the lightcurve (see Fig.4). However, the duration of the evolution is comparable. The timescale is, indeed,  $\approx 20$  days for SN 2008D and  $\approx 12$  days for SN 2015ap. This raises an interesting point toward the possibility that SN 2015ap could be characterized by a long duration short breakout phase, which is linked to the inflated envelope model suggested in Moriya et al. (2015).

### 3.1.2. Color evolution

Using the interpretation suggested in Yoon et al. (2019), the trend of the color evolution shown in Figure 3 is interpreted as an indication of the presence of a binary system. The results in Yoon et al. (2010) and Moriya et al. (2015) provide a set of criteria to distinguish between single-star and binary-star systems. The inflated envelope model for WR progenitors can indeed alter the shock breakout and be responsible for the variation in the rising phase of the SN light curve. A mass loss history model that can justify this kind of evolution typically involves the presence of a companion star in a binary system, which pushes the WR star to its Eddington limit by accreting its outer envelope

material. This can be outlined by examining the color evolution of the SN light curve. The color curve in the early stages of a SN Ib/Ic can provide information on the degree of mixing of the  $^{56}\text{Ni}$  in the ejected materials. Specifically:

- A weak mixing of the  $^{56}\text{Ni}$  leads to a color curve characterized by three phases: rapid initial reddening, a reversal toward blue due to heating of the  $^{56}\text{Ni}$ , and finally a return to red until the nebular phase.
- Strong mixing of the  $^{56}\text{Ni}$ , on the other hand, suppresses the reversion phase toward blue and leads to a monotonous evolution of the color curve.

The trend observed in color evolution of SN 2015ap has been observed in SNe such as SN 1999ex, SN 2008D, and iPTF13bvn, and the differences in mixing suggest a different origin of the progenitors. In particular, Yoon et al. (2019) suggests that the progenitors of SN Ib and SN Ic differ in terms of He content and mixing of the  $^{56}\text{Ni}$ . The model with a binary progenitor is compatible with weak mixing of the  $^{56}\text{Ni}$ , since mass transfer can remove part of the outer layers without strong mixing of the radioactive elements in the upper layers of the envelope.

### 3.2. Light curve modelling

In Prentice et al. (2018b) and Aryan et al. (2021) SN 2015ap is described as a He-rich supernova with a photospheric velocity near maximum light  $\approx 9000 \text{ km s}^{-1}$ . With the known values of the photospheric velocity near maximum light,  $t_{\text{rise}}$ , and a constant opacity  $\kappa = 0.07 \text{ cm}^2 \text{ g}^{-1}$ , Aryan et al. (2021) also obtain an ejecta mass  $M_{\text{ej}} = 2.2 \pm 0.6 M_{\odot}$  and kinetic energy  $E_k = 1.05 \pm 0.31 \times 10^{51} \text{ erg}$  from the Arnett (1982) model with a  $M_{^{56}\text{Ni}} = 0.14 \pm 0.02 M_{\odot}$ .

We used simple light curve modeling to estimate the ejecta mass of SN 2015ap using the Modular Open Source Fitter for Transients (MOSFiT; Guillochon et al. 2018). MOSFiT is a publicly available code that we employed to fit semianalytic models to the multiband observed light curves of SN 2015ap. All model fitting was performed using the dynamic nested sampler DYNESTY package (Speagle 2020) option in MOSFiT.

Figure 5 and Table 2 show the results from the fitting procedure assuming all parameters are unbound.

We compare the models in Table 1 using the Watanabe-Akaike Information Criterion (WAIC), a statistical measure that scores Bayesian models. It estimates the average predictive log-likelihood while accounting for model complexity and data variability. WAIC is preferred over the Aikake Information Criterion (AIC) in Bayesian contexts because it considers the entire posterior distribution rather than a single point estimate (Watanabe 2010).

Considering just the WAIC, the CSM model appears as the best model in describing SN 2015ap photometry. However, looking at the predicted evolution of the light curve, it can be noted that the rise of the SN as its maximum is not reliable, as for the last part of the tail. This findings suggest that other sources are powering the SN.

In all cases, the observed features are not entirely matched by the models. The magnitude at maximum is accurately reproduced in both *magni* and *slsn* models across almost all bands. However, these models fail to account for the non-negligible fluctuations observed around the descending tail. Moreover, except for *magnetar* model, all the models underestimate the observed magnitudes during the rising phase and the late-phase tail. Hence, these results indicate the presence of an additional underlying mechanism.

Model name	Descriptions	References
csm	Interacting CSM-SNe	Chatzopoulos et al. (2013b)
magnetar	Magnetar engine with simple SED	Nicholl et al. (2017b)
magni	Magnetar engine with simple SED + NiCo decay	Nicholl et al. (2017b); Nadyozhin (1994)
sln	Magnetar + modified SED + constraints	Nicholl et al. (2017b)

**Table 1.** Description of the MOSFit models used for the model fitting

model name	$\frac{d_L}{\text{Mpc}}$	$\frac{B}{10^{14} \text{ G}}$	$\frac{M_{NS}}{M_\odot}$	$\frac{P_{Spin}}{10^{-3} \text{ s}}$	$\frac{M_{ejecta}}{M_\odot}$	$\frac{v_{ej}}{\text{km s}^{-1}}$	$\frac{M_{CSM}}{M_\odot}$	$f_{56\text{Ni}}$
csm	21.88	-	-	-	0.94	1995	0.83	-
magnetar	-	0.15	1.77	1.23	0.001	14791	-	-
magni	-	6.92	1.21	5.2	0.67	12022	-	0.44
sln	79.43	3.9	1.01	9.90	1.26	12104	-	-

**Table 2.** Model parameters from MOSFit. Uniform distributions are used as priors for all the parameters. Uncertainties on the parameters are the 10% of the best-fit values.

### 3.3. Spectra

The galaxy-subtracted spectral evolution of SN 2015ap is presented in Figure 6. We extracted the line intensity by subtracting the pseudo-continuum, which includes contributions from unresolved absorption/emission features, scattered light, and possible instrumental artifacts. The continuum model is constructed by fitting a linear model to the arbitrarily selected continuum region on both sides of the emission feature. We measured the line velocities using the flux-weighted centroid of the emission feature, without modeling its complex velocity structure with a Gaussian fit. The velocity uncertainties include contributions from flux errors and variations due to different choices of the continuum region. However, we did not account for systematic uncertainty from the unknown baseline of the line feature. We measured the velocities for all the isolated emission lines in the evolution of multi-epoch spectra. We avoided the lines that showed the P-Cygni profile which inherited a complex structure that bias the measure. We used `specutils` package to analyze spectral data. The results are shown in Figure 6. To be sure we properly excluded galaxy contribution, we measured the  $H_\alpha$  luminosity evolution with time. We were mainly interested in the  $H_\alpha$  line, due to its link with accretion phenomena, which in our case can indicate the presence of a companion.  $H_\alpha$  luminosity evolution matched the trend of SN 2015ap bolometric’s lightcurve evolution indicating that the emission we are measuring comes from the region of the ejecta itself.

The early-time spectra show a blue continuum, which is characteristic of high-energy events like supernova explosions. This blue shift indicates that the ejecta are moving away from the observer at high velocities. Zooming around the iron absorption line (Fig. 16 in Gangopadhyay et al. 2020) it is visible a ‘W’ Shape Absorption Feature: the spectra taken at 5 and 7 days post-explosion reveal a ‘W’-shaped absorption feature around 4000 Å, which is associated with Fe complexes.

The spectral features, including the ‘W’ shape, suggest that the progenitor of SN 2015ap is likely a star with a mass between 12 and 20  $M_\odot$ . This estimation is supported by the analysis of the [O I]/[Ca II] ratio and nebular spectral modeling, which indicate a low-mass star in a binary system (Kuncarayakti et al. 2015). The [O I]/[Ca II] ratio is a significant diagnostic tool in determining the progenitor mass. In the case of SN 2015ap, this ratio is approximately 0.71, which is consistent with low-mass progenitors in binary systems. This ratio is influenced by various factors, including temperature and density, and serves as a demarcation between binary and single progenitor systems. Using

the relation:

$$M_O = 10^8 f([\text{OI}]) D^2 e^{\frac{2.28}{T_4}}$$

where  $M_O$  is the mass of the neutral O in  $M_\odot$  units,  $D$  is the distance to the galaxy in Mpc,  $f([\text{OI}])$  is the total flux of the [OI] 6300, 6364 Å feature in  $\text{ergs}^{-1}\text{cm}^{-2}$ , and  $T_4$  is the temperature of the O-emitting region in units of  $10^4$  K. Using the observed flux of  $4.0 \times 10^{-15} \text{ ergs}^{-1}\text{cm}^{-2}$  of the [OI] 6300, 6364Å doublet from 57389.08 MJD spectrum, and adopting  $T_4 = 0.37$  K, we estimate  $M_O \approx 0.47 M_\odot$ . With the assumption that at most the 50% contribute to the emission, we estimate that the total amount of Oxygen should not exceed  $0.9 M_\odot$ . The nebular spectral modeling in Gangopadhyay et al. (2020) indicates that the progenitor is most likely a star in the range of 12 to 17  $M_\odot$ , with a strong likelihood of being in a binary association. This modeling takes into account the observed line luminosities and the overall spectral characteristics.

The indication that SN 2015ap’s progenitor is a massive-mass star in a binary system has important implications for its evolution. In binary systems, mass transfer can occur, affecting the final mass and composition of the progenitor star before it undergoes a supernova explosion. This interaction can lead to the stripping of outer layers, resulting in the stripped-envelope nature of Type Ib supernovae like SN 2015ap. SN 2015ap shows an interesting feature of  $H_\alpha$ , characterized by a very narrow feature on top of a broader one, the wavelength range of interest in the supernova spectrum could be contaminated by host galaxy emission from nearby H II regions. However, checking the spectra of the host at different epochs, we confirm that the narrow feature does not come from any artifact due to host galaxy line contamination. Bottom panel in Figure 6 shows the narrow feature shows back-and-forth shifts in wavelength, meaning, moving to shorter and longer wavelengths around the rest-wavelength of  $H_\alpha$ . The shifting behaviour shows a cyclical pattern, consistent with the 7.8-day period as derived for the periodic modulation in the optical light curves (see Figure 7).

Similarly to SN 2022jli (Chen et al. 2024a), we interpret the periodic undulation in the SN 2015ap light curve coming from a limited region with relatively small size in the center of the ejecta. This implies, similarly, the emission of  $H_\alpha$  also comes from the center of the ejecta. The hydrogen responsible for the  $H_\alpha$  emission likely originates from the companion star’s envelope, which is accreted onto the newly formed compact object.  $H_\alpha$  emission lines have been commonly observed in binary systems with accretion disks, which could serve as an analogy in the

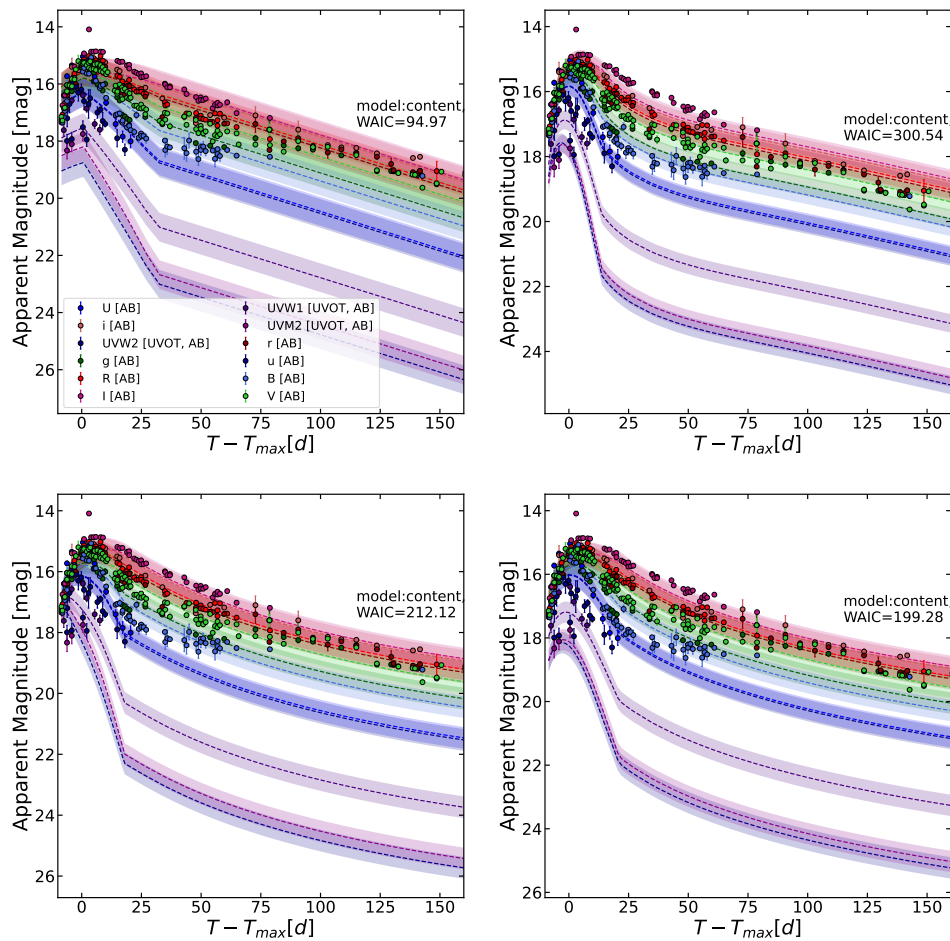


**Fig. 5.** Light curve modeling for SN 2015ap with different power source scenarios as described in Table 1. For more detail on the analysis see Sect. 3.2.

low accretion rate regime to understand the emission mechanism and structure of the  $H_\alpha$  in SN 2015ap as in SN 2022jli.

The overall assumption is the orbital velocity is interpreted as the major component. We need to point out that other possible kinematic processes may complicate the velocity evolution, such as: the velocity structure of the accretion disk, the mass flow from the companion star to the compact object, and the outflow of winds. The potential eclipse of the accretion disk by the companion star and the emission from the companion envelope could also complicate the velocity structure of the  $H_\alpha$  emission line.

### 3.4. Periodic Variability

SN 2015ap appears as a typical type-Ib SN. A closer inspection of the light curve (Figure 1) after the peak reveals the presence of photometric fluctuations. These modulations are visible with similar amplitude in all the available bands, and across different telescope and instrument combinations, indicating that this is neither an instrumental nor a calibration effect.

To identify and quantify potential periodicity, we first subtracted the decline trend from the light curve. To separate the contribution of the decline due to  $^{56}\text{Ni}$  from the modulation we applied a wavelet decomposition, which has been performed using the python pywt package (Lee et al. 2019). Hence, we extrapolated the lowest-order component that describes the large-scale structure of the light curve. The modulation contribution in the photometric evolution comes from subtracting the large-scale structure from the light curve.

A Lomb-Scargle analysis would generally be better suited for highlighting the presence of periodicity in a time series. However, the limited data on the light curve’s decay tail, combined with the heteroscedastic distribution of the data over time during the later stages of the SN evolution, introduces bias in the analysis. This is because a proper definition of the Nyquist frequency is impossible under these conditions. Thus, we performed as a first-order analysis an autocorrelation analysis to highlight the presence of a periodic behavior in the data. The analysis of the Autocorrelation Function (ACF) has revealed the presence of a significant periodicity of  $6.0 \pm 0.8$  days, with a

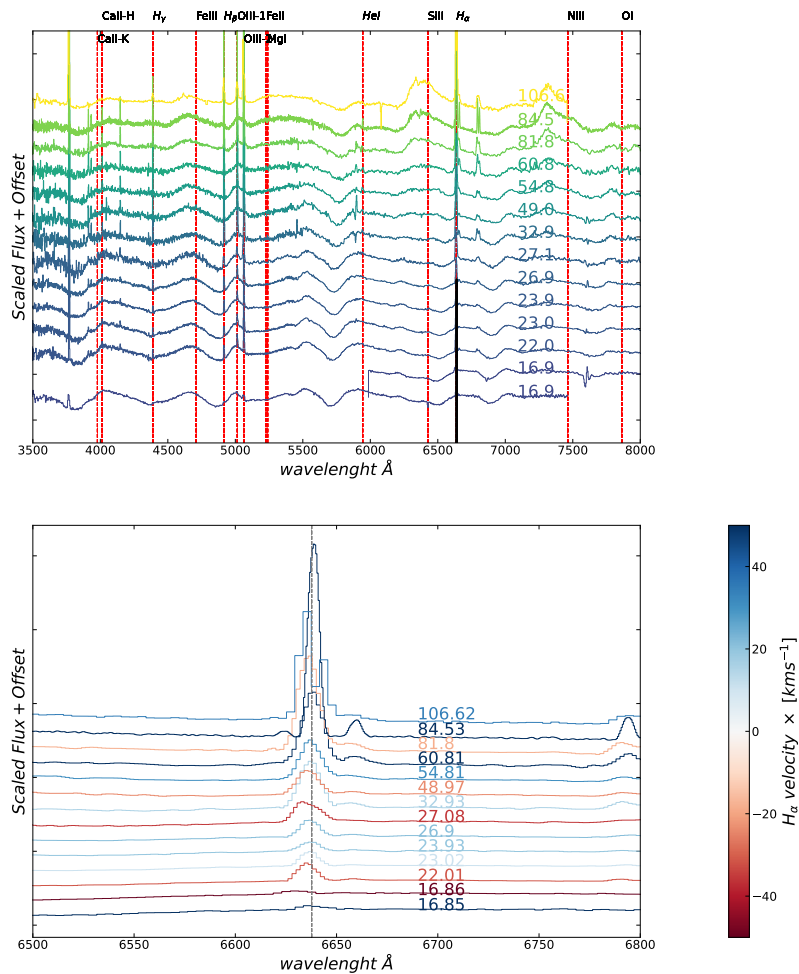


**Fig. 6.** Multi-epochs spectra of SN 2015ap (top panel) color coded with respect to the temporal evolution of the spectra in MJD; and a zoom of the  $H_\alpha$  line color coded with its velocity (bottom panel). It appears that the peak line velocities vary periodically through the entire evolution of the spectra (bottom panel). The labels of the phase that appear on the right side of all the spectra are estimated with respect to the very first available photometric observation.

probability of 95% to find the measured value within the uncertainty region (see Fig. 8). This periodicity corresponds to the most prominent peak of the ACF, indicating a recurring variability in the source. The result is consistent across different bands, suggesting that the periodic behavior is independent of wavelength.

The detection of periodic signals in irregularly sampled time series is a fundamental challenge in astronomy, as traditional methods such as the Lomb-Scargle periodogram often struggle with poorly defined statistical properties under uneven sampling. In particular, when stochastic variability (e.g., red noise) is present, standard techniques tend to overestimate the significance of periodic signals, increasing the likelihood of false positives. To address these issues, we adopted a Gaussian Process (GP)-based approach as described in Gúrpide & Middleton (2025), which provides a flexible probabilistic framework for modeling time series data while explicitly accounting for tem-

poral correlations. Unlike Fourier-based methods, GP modeling operates directly in the time domain, ensuring a well-defined likelihood function that can be leveraged for hypothesis testing.

Hence, we considered a Bayesian approach to deeply scan the parameters space of a periodic-based Gaussian Process. We extracted periodicity measurement from the posterior distribution of the parameter space of a periodic kernel

$$k(x_i, x_j) = \exp\left(-\frac{2 \sin^2(\pi d(x_i, x_j)/p)}{l^2}\right).$$

where  $l$  is the length scale of the kernel,  $p$  is the periodicity of the kernel and  $d(\cdot, \cdot)$  is the Euclidean distance.

We populated the posterior through the Monte Carlo Markov Chain method (for details see, e.g., Speagle 2019, and references therein.), implemented in emcee python package (Foreman-Mackey et al. 2013). For all the filters the period associated with the peak of the distribution is  $P \approx 8.41 \pm 0.80$  d (see Figure B.1).

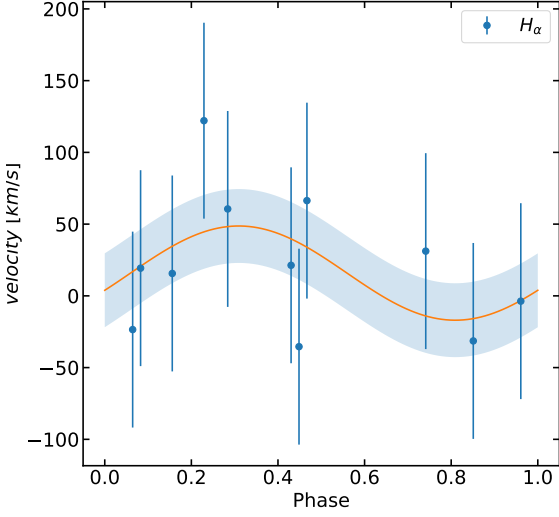


**Fig. 7.** The phase folded velocity curve of  $H_\alpha$  line.

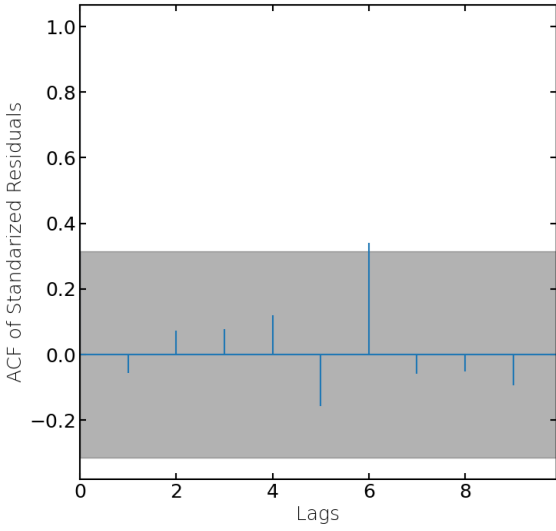


**Fig. 8.** The auto-correlation function of the standardized residuals. The shaded areas indicate the 95% confidence level expected for white noise. Lags are expressed in days.

The comparison between the best fit and the data is presented in Figure 9, apart from the phase differences due to the timescales of the emission in the different bands the trend is similar in all the filters. However, the paucity of data is evident and this could have caused a spurious detection of a periodicity due to noise. By constructing likelihood ratio tests (LRT) using posterior distributions derived from the inferred noise properties, we robustly assess the significance of candidate periodic signals while minimizing the risk of misidentification (see Fig. 10). We inferred the improvement in adding the periodic model simulating 1000 time series from the posterior distribution of the noise and measuring the LRT with respect to the periodic model. The observed  $T_{LRT}$  is 6.9, which falls in the outer region of the dis-

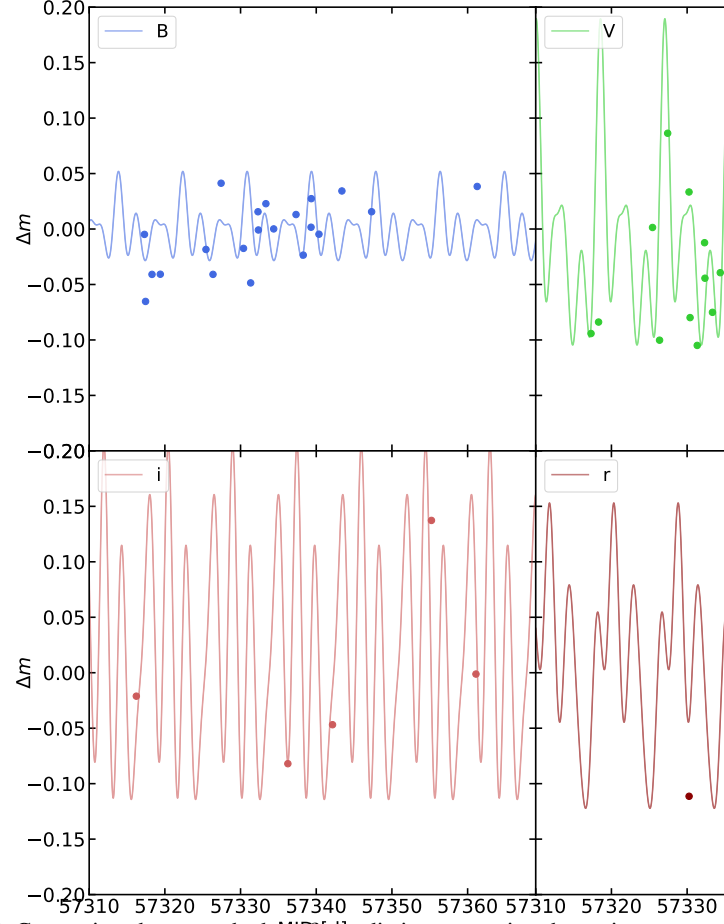


**Fig. 9.** Comparison between the best fit predictions assuming the periodic model and the observed data.

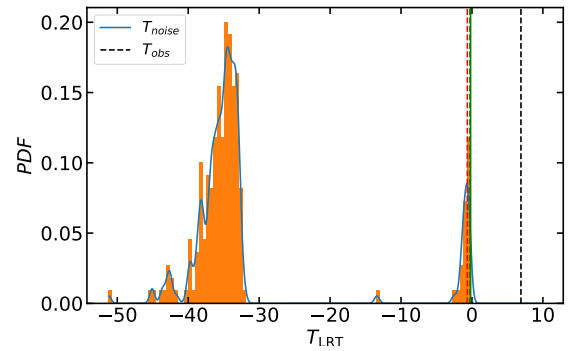


**Fig. 10.** Reference LRT distribution generated from simulated light curves from the posteriors of the null hypothesis. The solid orange line shows a fit to the distribution using a log-normal. The  $T_{LRT}$  observed in the data is shown as a dashed black line.

tribution, assessing that adding the periodic signal significantly improves the model, suggesting that the periodicity is real.



## 4. Discussion

The data presented in this paper appear similar to those of SN 2022jli (Moore et al. 2023), with the bolometric light curve peaking at higher energy than typical SE-SNe, and the rising rate being faster than in other similar SNe, yet comparable to SN 2022jli. The most interesting similarity is the presence of a periodic modulation in both photometry and spectra. Therefore, the case of SN 2015ap underlies a physical phenomenon responsible for the periodic fluctuations, which could be related to SN 2022jli. In this section, we discuss the possible scenarios that could explain the periodic variability observed in SN 2015ap.

### 4.1. Interaction with CSM

The ejecta-CSM interaction is one of the main mechanisms for SN light curve re-brightening (e.g., Tartaglia et al. 2016; McDowell et al. 2018; Suzuki et al. 2019; Sollerman et al. 2020; Pellegrino et al. 2022). However, the presence of multiple bumps with a time periodicity requires an ad-hoc CSM distribution like, for instance, concentric shells lost by the progenitor in the late phases of its evolution. During the undulations, SN 2015ap brightens up to  $\approx 10^{42}$  erg s $^{-1}$  for  $\approx 8$  days. Using the scaling relation  $L = \frac{1}{2} M_{CSM} v^2 / t_{rise}$  (Smith & McCray 2007; Quimby et al. 2007; Nicholl et al. 2016), we estimated the mass required to account for the bump to be  $M_{CSM,bump} \approx 1.5 \times 10^{-2} M_{\odot}$ , assuming  $v = 11200$  km s $^{-1}$  from Fe II line velocity measurements, and  $t_{rise} = 5.4$  days. The average pre-explosion mass-loss rate needed to produce this CSM mass per shell can be calculated by setting  $\frac{\dot{M}}{v_w} = \frac{M_{CSM,bump}}{\Delta R}$ , where  $v_w$  is the wind velocity and  $\Delta R = vt_{bump}$  is the radial distance bounding this CSM mass. For an ejecta velocity  $v = 11800$  km s $^{-1}$  (value taken from the fitting procedure described in subsection 3.2) and  $t_{bump} = 7.8$  days, this gives  $\dot{M} = 2 \times 10^{-6} \frac{v_w}{1000 \text{ km s}^{-1}} \frac{M_{\odot}}{\text{yr}}$ . This is consistent with the mass-loss rates observed from WR stars (e.g, Sander & Vink 2020), suggesting that a “typical” wind mass-loss rate could potentially provide the CSM structure needed to explain the periodic modulation of SN 2015ap.

Nested dust shells caused by colliding winds in the massive binary system WR140 have been spectacularly revealed by JWST imaging (Lau et al. 2022). These 17 observed shells form due to repeated dust formation episodes every 7.93 years, triggered by the periastron passage of the companion O5.5fc star orbiting the WC7 Wolf-Rayet star. If SN 2015ap’s modulations were due to density peaks in the CSM similar to WR140 shells, the binary progenitor would need to eject these shells approximately 400 times more frequently. A stronger argument against this scenario involves the ejecta velocity (11800 km s $^{-1}$ ) and the 7.8-day periodicity of SN 2015ap. This yields a shell separation of approximately 6 Astronomical Units (AU, which is three orders of magnitude smaller than the 4400 AU observed in WR140. Hence, for the progenitor system of SN 2015ap, shells would need to be ejected roughly every  $\approx 40$  days, which is highly unrealistic compared to the 8-year ejection period in WR140.

### 4.2. Ejecta-Companion interaction

The periodicity in both photometry and spectra evolution suggests that a possible scenario involves a binary system to set the clock of the bumps. The luminosity of H $_{\alpha}$  emission follows the evolution of the bolometric luminosity,  $L_{H_{\alpha}} = 0.004 \times L_{bol}$ . This implies the same origin for the H $_{\alpha}$  emission as for the luminos-

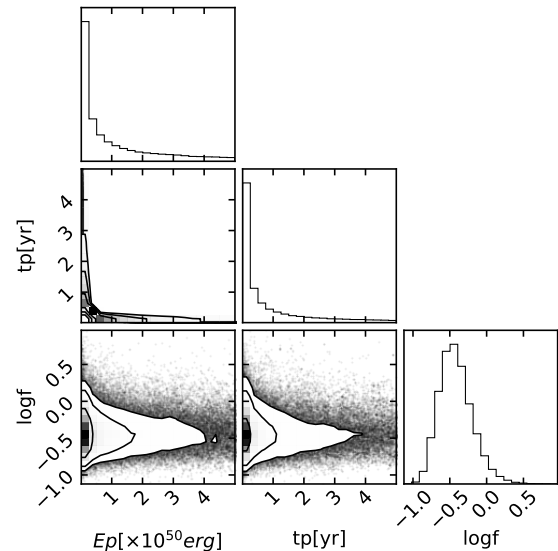


**Fig. 11.** Corner plot from the fitting procedure of the late evolution of the light curve described in subsection 4.3.

ity excess of the SN, suggesting that the source of this line also comes from the central region of the system.

Hence, a companion star with a hydrogen-rich envelope is necessary to provide the hydrogen, which supports the existence of a binary system. Such a binary system provides direct evidence supporting the binary origins of some SE-SNe.

Due to the presence of O lines in the spectra at almost all epochs, it is expected for the progenitor of SN 2015ap to be a WR star, specifically a WO star. Considering this possibility, the scenario where the progenitor of SN 2015ap was part of a binary system is supported by the recent discovery in Anastasopoulou et al. (2024), where it is shown that the majority of WR stars are expected to be part of a binary system.

Another point that supports this scenario is that the observed bumps have a short timescale, a constant profile, and a stable ratio to the continuum flux. This suggests that the fluctuating light is not diluted even as the ejecta expands. To achieve this, the emitting region must cover a consistent fraction of the expanding ejecta. To maintain coherence, the power source should be located near or in the center of the ejecta. For the bump profile to rise quickly, optical photons must diffuse through the ejecta in less than 3 days.

This scenario would explain the modulation of the light curve as the companion star would be inflated due to heating from the SN ejecta-companion interaction, and the inflated portion of the envelope may interact with the NS, causing periodic accretion on the timescale of the orbital period.

The effect of envelope inflation is not limited to the breakout phase. Subsequently, the diffused light continues to shape the early rise of the SN light curve, extending its duration and altering its morphology compared to standard models. Notably, the presence of an inflated envelope can introduce distinct bumps or plateaus in the early light curve as the shock-heated material in the extended layers gradually releases its energy. These features have been observed in several SNe and are often attributed to additional sources of interaction, such as CSM.

However, in the case of Wolf-Rayet (WR) stars with inflated envelopes, these bumps can arise intrinsically from the structure of the progenitor itself without requiring dense CSM interaction. Additionally, the presence of an extended envelope affects the

thermal properties of the shock breakout emission. The diffusion of photons through the low-density envelope can lead to sudden temperature variations, particularly in regions associated with the observed bumps. As the shock front propagates through the inflated structure, its temperature evolution deviates from the standard expectation for compact progenitors. In particular, the initial breakout phase may show a lower-than-expected temperature due to the extended diffusion time, followed by transient heating episodes as different layers of the envelope contribute to the observed emission.

An argument against this scenario is the gradual in-spiraling of the NS into the companion, as predicted by Hirai & Podsiadlowski (2022). However, in the case of the inflated companion, the low-density envelope results in a slower orbital decay (Hirai et al. 2018; Ogata et al. 2021).

The accreting compact object model can be thought of as an internal powering source. The energy released must diffuse through the ejecta on timescales determined by the opacity, density, and radius of the optically thick material. Hosseinzadeh et al. (2022) propose that a central origin is disfavored if the dimensionless depth of the powering source,  $\delta = \frac{t_{bump}\Delta t_{bump}}{t_{rise}^2}$  is significantly less than unity. With  $\Delta t_{bump}=7.8$  days and  $t_{rise}=30$  days, this parameter ranges between 0.3 and 1.35 for the earliest and latest bumps. This would favour a central, internal powering source, although Hosseinzadeh et al. (2022) note that the above expression is quite approximate and should only be treated as an order-of-magnitude result.

### 4.3. Highly magnetized compact object

The Ejecta-Companion interaction scenario, which seems the most favorable, takes into account only the gravitational interaction between the newly formed NS and the companion. However, it is not unlikely that a very strong magnetic field is present during the early phases of NS formation (Hirai & Podsiadlowski 2022). Gofman & Soker (2019) propose two outcomes for this scenario. Firstly, a double-phase evolution of the magnetic field may occur. In this configuration, a highly magnetized, newly born NS with a magnetic field of  $B \approx 10^{15}$  G evolves through jet activity on a time scale of  $10^4$  s. If jets are launched, they could transport the angular momentum of the accreted material, allowing the crust to form and the NS to relax. The second phase, once the newly born NS has relaxed, would be characterized by a magnetic field of  $B \approx 10^{13}$  G and a rotation energy of the order of  $E_p \approx 10^{50}$  erg. However, this double-phase evolution appears to be in contradiction with the constraints on the jet production suggested by García et al. (2014), who state that the magnetic field intensity required for jet production would cause the jets to form on a timescale of  $10^8$  years, making jet production highly improbable. The alternative scenario considers that a highly magnetized NS at birth could power a SN to reach a maximum luminosity of:

$$L_{peak} \approx f \frac{E_p t_p}{t_d^2} \left[ \ln \left( 1 + \frac{t_d}{t_p} \right) - \frac{t_d}{t_p + t_d} \right],$$

where  $E_p \approx 2 \times 10^{50} \left( \frac{I_{NS}}{10^{45} \text{ g cm}^{-2}} \right) \left( \frac{P}{10 \text{ ms}} \right)^{-2}$  erg is the rotational energy of the NS,  $f$  is a correction fraction,  $t_d = \left( \frac{3\kappa M_{ej}}{4\pi v_{ej} c} \right)^{\frac{1}{2}}$  is the photon diffusion time scale, and  $t_p = 0.44 \left( \frac{P}{10 \text{ ms}} \right)^2 \left( \frac{B}{10^{14} \text{ G}} \right)^{-2} \left( \frac{I_{NS}}{10^{45} \text{ g cm}^{-2}} \right) \left( \frac{R_{NS}}{12 \text{ km}} \right)^{-4}$  yr is the spin-down time scale. In the previous equations,  $P$  refers to the

spin-down oscillation period. At late times after peak luminosity, the SN light curve follows the spin-down power

$L_p(t) = E_p t_p^{-1} \left( 1 + \frac{t}{t_p} \right)^{-2}$ . By fitting the late-time light curve of SN 2015ap to  $L_p(t)$  (see Figure 11), we find that a highly magnetized NS with an initial spin period of  $P = 2.01 \pm 1.34$  ms and an initial magnetic field of  $B = (6.73 \pm 0.01) \times 10^{14}$  G can produce the observed average luminosity and time-scale. These values appear in agreement with the best-fit values from light curve modeling with `Mosfit` subsection 3.2. Rapidly rotating NSs with a strong magnetic field in a binary system can accrete material from a companion through a magnetic gating process (Spruit & Taam 1993). When the magnetosphere is Rayleigh-Taylor stable, the gate is closed in the sense that plasma enters the magnetosphere only slowly via the cusps, diffusion, and magnetic reconnection. When the magnetosphere is driven Rayleigh-Taylor unstable by cooling of the external atmosphere and the resulting increase in the density of the plasma outside the magnetopause (the boundary between a NS's magnetosphere and the surrounding plasma environment), the gate opens in the sense that plasma rapidly enters the magnetosphere and accretes onto the NS surface at a high rate, producing increased X-ray emission. When the X-ray emission interacts with the ejecta, X-rays can be entirely absorbed by the ejecta that will re-emit the radiation at optical wavelengths.

To verify if gating mechanisms can be the instability process that triggers the periodic accretion the co-rotating radius of the binary system has to be approximately equal to the magnetosphere radius. Using the formalism in Littlefield et al. (2022) and assuming the magnetic field, the orbital period and the spin period estimated for the binary system of the SN 2015ap progenitor, we get:  $R_M = 1.4 \times 10^{10} \left( \frac{\dot{M}}{10^{15} \text{ g s}^{-1}} \right)^{-\frac{2}{7}} M_{NS}^{\frac{1}{7}} \left( \frac{\mu}{10^{32} \text{ G cm}^3} \right)^{\frac{4}{7}} \text{ cm} = O(10^9 \text{ cm})$ ,  $R_{cor} = 3.52 \times 10^{10} M_{NS}^{\frac{1}{2}} P_{spin}^{\frac{2}{3}} \text{ cm} = O(10^9 \text{ cm})$ . Therefore, at least theoretically, the magnetic gating model appears to be the best candidate to explain the periodicity of SN 2015ap.

One critical issue that remains unsolved is the onset of a high magnetic field on the newly born NS. However, the recent work of Barrère et al. (2022) suggests that it is not so unlikely for newly born NS to amplify their initial magnetic field due to the accretion of fall-back material from the ejecta through the Tayler-Spruit dynamo loop.

## 5. Conclusions

We have presented detailed, multi-wavelength, high-cadence observations of Type Ib SN 2015ap. This supernova appears to be very peculiar due to exceptionally high bolometric peak magnitude, connected to high explosion energy, and the presence of modulation in the tail of its light curve. To better investigate these features, we analyzed both photometry and spectra. The analysis of the magnitude residuals indicates that the light modulation can be described by a sinusoidal pattern with a period of  $8.4 \pm 0.8$  days. The analysis of SN 2015ap suggests that its observed periodicity in both photometry and spectral evolution can be naturally explained within a binary system scenario. The presence of a hydrogen-rich companion star is a plausible explanation for the source of  $H_\alpha$  emission and the luminosity excess. The observed short-timescale bumps and their stable characteristics further support the idea of an internal power source, likely linked to the ejecta-companion interaction.

Additionally, the presence of a highly magnetized compact object, such as a newly formed neutron star, could provide an al-

ternative or complementary mechanism to explain the observed luminosity variations. The spin-down of a rapidly rotating neutron star with a strong magnetic field aligns with the late-time evolution of the light curve, as confirmed by our modeling.

Overall, the combination of these factors strengthens the hypothesis that SN 2015ap originated from a binary progenitor system, highlighting the role of binary interactions in shaping the evolution of stripped-envelope supernovae. Future observations of similar systems will be crucial in further constraining these scenarios.

## 6. Acknowledgement

This work was initially thought out and developed at The Unconventional Thinking Tank Conference 2022, which is supported by INAF. We thank F. Patat, S. Ascenzi, and A. Papitto for fruitful discussions that improved the manuscript and that helped in the interpretation and analysis of the event. This work was supported by the Preparing for Astrophysics with LSST Program, funded by the Heising Simons Foundation through grant 2021-2975, and administered by Las Cumbres Observatory. We acknowledge support from INAF Minigrant (Research Grant ‘KeNSHIRO: KNe Serendipitous Hunt In the Rubin Observatory era’).

## References

- Agudo I., et al., 2023, *A&A*, 675, A201  
 Anastasopoulou K., et al., 2024, arXiv e-prints, p. arXiv:2408.11087  
 Arnett W. D., 1982, *ApJ*, 253, 785  
 Arnett W. D., Fu A., 1989, *Astrophysical Journal*, Part 1 (ISSN 0004-637X), vol. 340, May 1, 1989, p. 396-425., 340, 396  
 Aryan A., et al., 2021, *Monthly Notices of the Royal Astronomical Society*, 505, 2530  
 Astropy Collaboration et al., 2013, *A&A*, 558, A33  
 Astropy Collaboration et al., 2018, *AJ*, 156, 123  
 Astropy Collaboration et al., 2022, *ApJ*, 935, 167  
 Barrère P., Guilet J., Reboul-Salze A., Raynaud R., Janka H. T., 2022, *A&A*, 668, A79  
 Branch D., et al., 2002, *The Astrophysical Journal*, 566, 1005  
 Brown T. M., et al., 2013, *PASP*, 125, 1031  
 Brown P. J., Breeveld A. A., Holland S., Kuin P., Pritchard T., 2014, *Ap&SS*, 354, 89  
 Chatzopoulos E., Wheeler J. C., Vinko J., Horvath Z. L., Nagy A., 2013b, *ApJ*, 773, 76  
 Chatzopoulos E., Wheeler J. C., Vinko J., Horvath Z. L., Nagy A., 2013a, *The Astrophysical Journal*, 773, 76  
 Chen P., et al., 2024a, *Nature*, 625, 253–258  
 Chen P., et al., 2024b, *Nature*, 625, 253  
 Chengalur J. N., Salpeter E. E., Terzian Y., 1993, *ApJ*, 419, 30  
 Chevalier R. A., 1982, *ApJ*, 258, 790  
 Chevalier R. A., Fransson C., 1994, *ApJ*, 420, 268  
 Chini R., Hoffmeister V. H., Nasserl A., Stahl O., Zinnecker H., 2012, *Monthly Notices of the Royal Astronomical Society*, 424, 1925  
 Claeys J., De Mink S., Pols O., Eldridge J., Baes M., 2011, *Astronomy & Astrophysics*, 528, A131  
 De Cuyper J.-P., 1982, *International Astronomical Union Colloquium*, 69, 417–443  
 Eldridge J. J., Izzard R. G., Tout C. A., 2008, *MNRAS*, 384, 1109  
 Eldridge J. J., Fraser M., Maund J. R., Smartt S. J., 2015, *MNRAS*, 446, 2689  
 Eldridge J. J., Stanway E. R., Xiao L., McClelland L. A. S., Taylor G., Ng M., Greis S. M. L., Bray J. C., 2017, *PASA*, 34, e058  
 Elmhamdi A., Danziger I. J., Branch D., Leibundgut B., Baron E., Kirshner R. P., 2006, *A&A*, 450, 305  
 Filippenko A. V., 2005, in Turatto M., Benetti S., Zampieri L., Shea W., eds, *Astronomical Society of the Pacific Conference Series Vol. 342, 1604-2004: Supernovae as Cosmological Lighthouses*, p. 87  
 Filippenko A. V., Li W. D., Treffers R. R., Modjaz M., 2001, in Paczynski B., Chen W.-P., Lemme C., eds, *Astronomical Society of the Pacific Conference Series Vol. 246, IAU Colloq. 183: Small Telescope Astronomy on Global Scales*, p. 121  
 Fitzpatrick E. L., 1999, *PASP*, 111, 63  
 Foreman-Mackey D., Hogg D. W., Lang D., Goodman J., 2013, *PASP*, 125, 306  
 Gal-Yam A., 2017, *Observational and Physical Classification of Supernovae*. Springer International Publishing, Cham, pp 1–43, doi:10.1007/978-3-319-20794-0\_35-1, https://doi.org/10.1007/978-3-319-20794-0\_35-1  
 Gangopadhyay A., et al., 2020, *MNRAS*, 497, 3770  
 García F., Aguilera D. N., Romero G. E., 2014, *A&A*, 565, A122  
 Gofman R. A., Soker N., 2019, *MNRAS*, 488, 5854  
 Guillochon J., Parrent J., Kelley L. Z., Margutti R., 2017, *ApJ*, 835, 64  
 Guillochon J., Nicholl M., Villar V. A., Mockler B., Narayan G., Mandel K. S., Berger E., Williams P. K. G., 2018, *The Astrophysical Journal Supplement Series*, 236, 6  
 Gúrpide A., Middleton M., 2025, *Monthly Notices of the Royal Astronomical Society*, p. staf196  
 Hirai R., Podsiadlowski P., 2022, *Monthly Notices of the Royal Astronomical Society*, 517, 4544  
 Hirai R., Podsiadlowski P., Yamada S., 2018, *The Astrophysical Journal*, 864, 119  
 Hosseinzadeh G., Berger E., Metzger B. D., Gomez S., Nicholl M., Blanchard P., 2022, *The Astrophysical Journal*, 933, 14  
 Kasen D., Bildsten L., 2010, *The Astrophysical Journal*, 717, 245  
 Kasen D., Metzger B. D., Bildsten L., 2016, *ApJ*, 821, 36  
 Kuncarayakti H., et al., 2015, *A&A*, 579, A95  
 Kuncarayakti H., et al., 2023, *A&A*, 678, A209  
 Lau R. M., et al., 2022, *Nature Astronomy*, 6, 1308  
 Lee G. R., Gommers R., Waselewski F., Wohlfahrt K., Leary A., 2019, *Journal of Open Source Software*, 4, 1237  
 Li W. D., et al., 2000, in Holt S. S., Zhang W. W., eds, *American Institute of Physics Conference Series Vol. 522, Cosmic Explosions: Tenth Astrophysics Conference*, pp 103–106, doi:10.1063/1.1291702  
 Littlefield C., Lasota J.-P., Hameury J.-M., Scaringi S., Garnavich P., Szkody P., Kennedy M., Leichty M., 2022, *The Astrophysical Journal Letters*, 924, L8  
 Liu L.-D., Gao H., Wang X.-F., Yang S., 2021, *ApJ*, 911, 142  
 Lyman J. D., Bersier D., James P. A., Mazzali P. A., Eldridge J. J., Fraser M., Pian E., 2016, *Monthly Notices of the Royal Astronomical Society*, 457, 328  
 Maeda K., et al., 2007a, *ApJ*, 666, 1069  
 Maeda K., et al., 2007b, *The Astrophysical Journal*, 666, 1069  
 McDowell A. T., Duffell P. C., Kasen D., 2018, *The Astrophysical Journal*, 856, 29  
 Moore T., et al., 2023, *ApJ*, 956, L31  
 Moriya T., Tominaga N., Blinnikov S. I., Baklanov P. V., Sorokina E. I., 2011, *MNRAS*, 415, 199  
 Moriya T. J., Sanyal D., Langer N., 2015, *A&A*, 575, L10  
 Nadyozhin D. K., 1994, *ApJS*, 92, 527  
 Nicholl M., 2018, *Research Notes of the AAS*, 2, 230  
 Nicholl M., et al., 2016, *ApJ*, 826, 39  
 Nicholl M., et al., 2017a, *ApJ*, 848, L18  
 Nicholl M., Guillochon J., Berger E., 2017b, *ApJ*, 850, 55  
 Ogata M., Hirai R., Hijikawa K., 2021, *MNRAS*, 505, 2485  
 Ostriker J. P., Gunn J. E., 1969, *ApJ*, 157, 1395  
 Pellegrino C., et al., 2022, *The Astrophysical Journal*, 926, 125  
 Podsiadlowski P., Joss P. C., Hsu J. J. L., 1992, *ApJ*, 391, 246  
 Prentice S. J., et al., 2018a, *Monthly Notices of the Royal Astronomical Society*, 485, 1559  
 Prentice S. J., Ashall C., James P. A., other 2018b, *Monthly Notices of the Royal Astronomical Society*, 485, 1559  
 Quimby R. M., Aldering G., Wheeler J. C., Höflich P., Akerlof C. W., Rykoff E. S., 2007, *The Astrophysical Journal*, 668, L99  
 Roming P. W. A., et al., 2005, *Space Sci. Rev.*, 120, 95  
 Ross T., et al., 2015, *Central Bureau Electronic Telegrams*, 4125, 1  
 Sana H., et al., 2012, *Science*, 337, 444  
 Sana H., et al., 2014, *ApJS*, 215, 15  
 Sander A. A. C., Vink J. S., 2020, *MNRAS*, 499, 873  
 Schlafly E. F., Finkbeiner D. P., 2011, *The Astrophysical Journal*, 737, 103  
 Schneider F. R. N., et al., 2014, *ApJ*, 780, 117  
 Shivvers I., et al., 2022, *VizieR Online Data Catalog: Berkeley sample of stripped-envelope SNe (Shivvers+, 2019)*, *VizieR On-line Data Catalog: J/MNRAS/482/1545*. Originally published in: 2019MNRAS.482.1545S  
 Smith N., McCray R., 2007, *The Astrophysical Journal*, 671, L17  
 Sollerman J., et al., 2020, *A&A*, 643, A79  
 Speagle J. S., 2019, arXiv e-prints, p. arXiv:1909.12313  
 Speagle J. S., 2020, *MNRAS*, 493, 3132  
 Spruit H. C., Taam R. E., 1993, *ApJ*, 402, 593  
 Sravan N., Marchant P., Kalogera V., Milisavljevic D., Margutti R., 2020, *ApJ*, 903, 70  
 Srinivasaragavan G. P., et al., 2024, *ApJ*, 960, L18  
 Stahl B. E., et al., 2019, *MNRAS*, 490, 3882  
 Stetson P. B., 1987, *PASP*, 99, 191  
 Sugimura K., Matsumoto T., Hosokawa T., Hirano S., Omukai K., 2020, *ApJ*, 892, L14  
 Suzuki A., Moriya T. J., Takiwaki T., 2019, *The Astrophysical Journal*, 887, 249

- Taddia F., et al., 2018, *A&A*, 609, A136  
Tartaglia L., et al., 2016, *Monthly Notices of the Royal Astronomical Society*, 459, 1039  
Utrobin V. P., Wongwathanarat A., Janka H.-T., Müller E., Ertl T., Menon A., Heger A., 2021, *The Astrophysical Journal*, 914, 4  
Watanabe S., 2010, arXiv e-prints, p. arXiv:1004.2316  
Woosley S. E., 2010, *ApJ*, 719, L204  
Yaron O., Gal-Yam A., 2012, *PASP*, 124, 668  
Yoon S.-C., Woosley S. E., Langer N., 2010, *The Astrophysical Journal*, 725, 940  
Yoon S.-C., Chun W., Tolstov A., Blinnikov S., Dessart L., 2019, *ApJ*, 872, 174  
Zapartas E., et al., 2017, *A&A*, 601, A29  
Zhang Z.-D., Yu Y.-W., Liu L.-D., 2022, *ApJ*, 936, 54

## Appendix A: Data curation

### Appendix A.1: Photometry

Data for SN 2015ap have been taken from different instruments and telescopes. Most of the publicly available data were downloaded from the Open Supernova Catalog (Guillochon et al. 2017) which refers to the multiepoch and multiwavelength detections used in Aryan et al. (2021). Ancillary data for the U, V, UVW1, UVW2, UVM2 bands were obtained from the Swift Optical/Ultraviolet Supernova Archive<sup>1</sup> archive. In addition, ugRri photometry (Prentice et al. 2018a) was obtained by the Las Cumbres Observatory (LCO; Brown et al. 2013) network of robotic telescopes. KAIT B, V, R, and I follow-up images of SN 2015ap were reduced using a custom pipeline detailed by (Stahl et al. 2019)).

Publicly available KAIT data were already post-processed by Aryan et al. (2021). They removed the host-galaxy background via image-subtraction procedures, using additional images obtained after the SN had faded below our detection limit. Point-spread-function (PSF) photometry was performed using DAOPHOT (Stetson 1987) from the IDL Astronomy User's Library.

For the B band maximum epoch, we adopt the estimate by Aryan et al. (2021)  $T_{max} = 57282.47 \pm 2.56$  MJD. Figure 1 shows the UuBVgRrli light curves of SN 2015ap, which are progressively broader and broader at longer wavelengths.

Distances are taken from the NASA Extragalactic Database (NED)<sup>2</sup>. For SN 2015ap, we corrected for Milky Way (MW) extinction using the values reported by NED (Schlafly & Finkbeiner 2011): 0.185, 0.154, 0.117, 0.092, and 0.064 mag for the U, B, V, R, and I bands, respectively.

To provide an overall description of the photometric behaviour of the object and to increase the signal-to-noise ratio, we derived the quasi-bolometric light curve. We made use of the `superbol` code (Nicholl 2018). The process can be summarised as follows. The extinction-corrected UuBVgRrli data are passed to `superbol`, which maps the light curve in each passband to a common time grid by interpolation and extrapolation. It then fits a blackbody to the spectral energy distribution (SED) at each epoch, up to the observed wavelength. Finally, the quasi-bolometric light curve is computed by trapezoidal integration.

The light curve morphology and photometric properties of SN 2015ap are described in Gangopadhyay et al. (2020), to which we refer the reader for more details.

### Appendix A.2: Spectroscopy

We present spectra spanning from 16 days to 100 days with respect to the B maximum. All spectra presented in this work have been obtained via the WISEREP repository (Yaron & Gal-Yam 2012). Galactic reddening was corrected using the dust extinction package of `astropy` (Astropy Collaboration et al. 2013, 2018, 2022) following the Fitzpatrick (1999) reddening law, the extinction-corrected spectra are shown in Figure 6, the spectral features of SN 2015ap reveal significant information about its composition and behaviour during its early phases. The main results from the spectra of this SN are shown in Gangopadhyay et al. (2020), the early spectra of SN 2015ap show strong ab-

sorption features of He I at various wavelengths, including 4471 Å, 5876 Å, 6678 Å, and 7065 Å.

The He I 5876 Å line exhibits an expansion velocity of approximately  $15500 \text{ km s}^{-1}$ . This high velocity is typical for stripped-envelope supernovae, suggesting a significant energy release during the explosion. In addition to He, the spectra also display prominent lines of other elements:

- Magnesium (Mg II): Lines of Mg II are observed, contributing to the overall spectral profile;
- Iron (Fe II): Fe II lines are present between 4100 and 5000 Å, indicating the presence of iron in the ejecta;
- Silicon (Si II): The Si II line is noted around 6250 Å, which is another common feature in Type Ib supernovae;
- Oxygen (O I): The O I 7774 Å line is also detected, further supporting the elemental composition of the supernova;

## Appendix B: Anylisys of periodicity by Gaussian Process regression

The analysis of periodic time series data using Gaussian Process (GP) models involves the application of the periodic kernel, a specialized covariance function that captures the inherent cyclic patterns in the data. The periodic kernel is a modification of the squared exponential (or Radial Basis Function, RBF) kernel, incorporating a sine function to ensure periodicity. This kernel is defined as:

$$k(x, x') = \sigma^2 \exp\left(-\frac{2 \sin^2\left(\frac{\pi(x-x')}{p}\right)}{l^2}\right)$$

where  $x$  and  $x'$  are two points in time,  $p$  is the period of the cycle,  $l$  controls the smoothness, and  $\sigma^2$  represents the variance.

When applying a Gaussian Process with this kernel to a dataset, the model infers a distribution over functions that are periodic with period  $p$ . This approach is particularly powerful for identifying and predicting cyclic behaviour in time series without requiring explicit knowledge of the underlying periodic structure. By optimizing the hyperparameters *e.g.*  $l$ , the GP can effectively capture the periodic nature of the data, making it useful in various applications. The flexibility of the GP framework allows it to accommodate uncertainty and noise in the data, providing not just a mean prediction but a full probabilistic description of the periodic process.

In Figure B.1 are shown the corner plot from the GP analysis of the period for the photometry of SN 2015ap.

<sup>1</sup> (SOUSA; <https://archive.stsci.edu/prepds/sousa/> Roming et al. 2005; Brown et al. 2014)

<sup>2</sup> <https://ned.ipac.caltech.edu/>

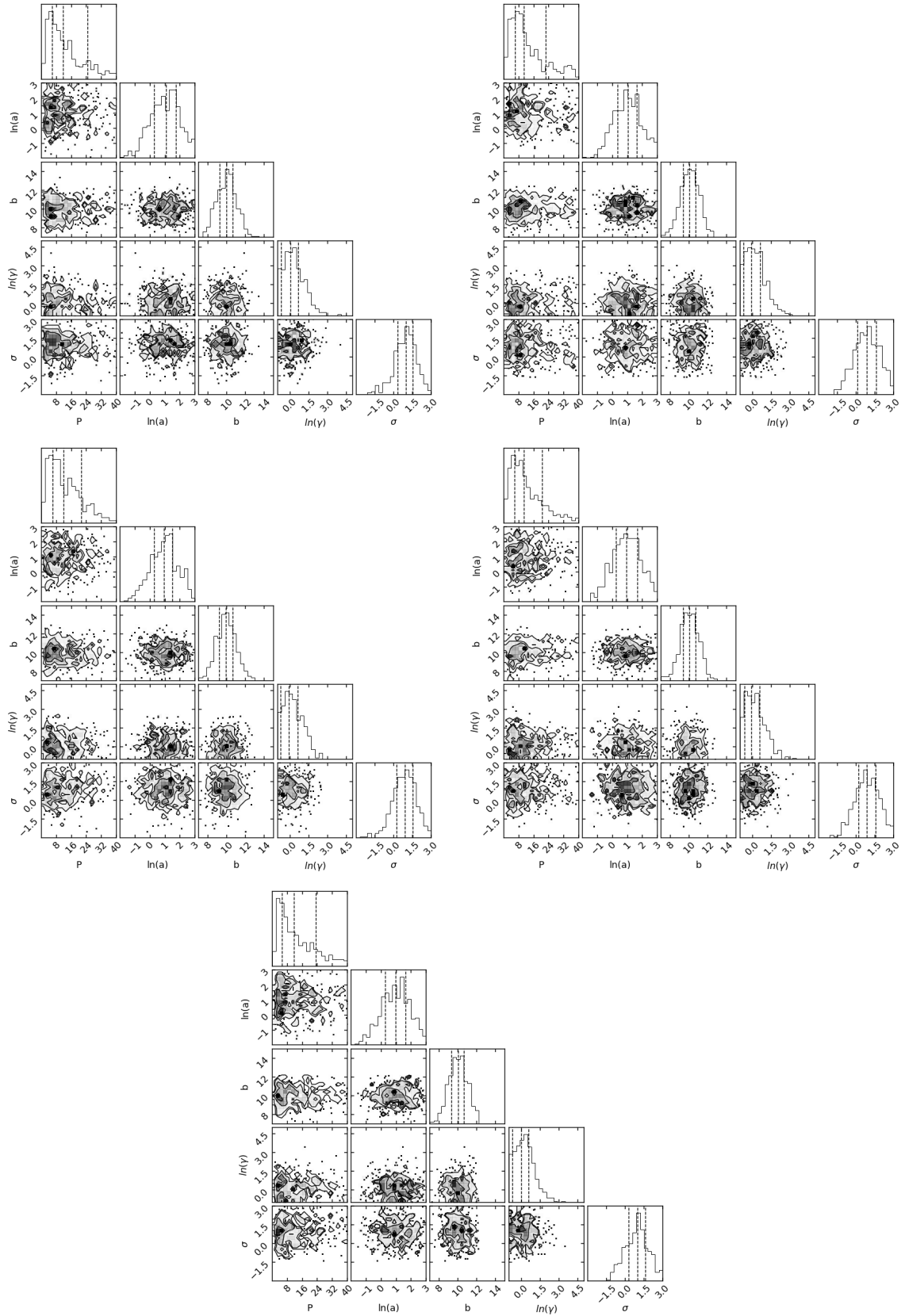


**Fig. B.1.** Results of the MCMC analysis for the regression parameters of the GP for the light curve residual, from top to bottom, of uBVrI filters.